SIBi
SISTEMA INTEGRADO DE BIBLIOTECAS
UNIVERSIDADE DE SÃO PAULO

Universidade de São Paulo

Biblioteca Digital da Produção Intelectual - BDPI

Departamento de Física e Ciência Interdisciplinar - IFSC/FCI

Artigos e Materiais de Revistas Científicas - IFSC/FCI

2010

Structural modeling of high-affinity thyroid receptor-ligand complexes

ORIGINAL PAPER

Structural modeling of high-affinity thyroid receptor–ligand complexes

Alexandre Suman de Araujo · Leandro Martínez ·
Ricardo de Paula Nicoluci · Munir S. Skaf ·
Igor Polikarpov

Abstract Understanding the molecular basis of the binding modes of natural and synthetic ligands to nuclear receptors is fundamental to our comprehension of the activation mechanism of this important class of hormone regulated transcription factors and to the development of new ligands. Thyroid hormone receptors (TR) are particularly important targets for pharmaceuticals development because TRs are associated with the regulation of metabolic rates, body weight, and circulating levels of cholesterol and triglycerides in humans. While several high-affinity ligands are known, structural information is only partially available. In this work we obtain structural models of several TR–ligand complexes with unknown structure by docking high affinity ligands to the receptors' ligand binding domain with subsequent relaxation by molecular dynamics simulations. The binding modes of these ligands are discussed providing novel insights into the development of TR ligands. The experimental binding free energies are reasonably well-reproduced from the proposed models using a simple linear interaction energy free-energy calculation scheme.

A. S. de Araujo · R. de Paula Nicoluci · I. Polikarpov
Instituto de Física de São Carlos, Universidade de São Paulo,
Av. Trabalhador SaoCarlense 400, IFSC, Grupo de
Cristalografia, P.O. Box 369, Sao Carlos, SP 13560-970, Brazil

L. Martínez · M. S. Skaf (✉)
Institute of Chemistry, State University
of Campinas-UNICAMP, P.O. Box 6154,
Campinas, SP 13084-862, Brazil
e-mail: skaf@iqm.unicamp.br

Introduction

The nuclear receptor (NR) superfamily is an important group of proteins that regulates the expression of genes related to organism development and metabolism control. It includes receptors for steroids, retinoids, fatty and bile acids, vitamin D, cholesterol metabolites, xenobiotics and thyroid hormones (Ribeiro et al. 1998, 1995; Weatherman et al. 1999; Yen 2001; Togashi et al. 2005). NRs transcription regulation relies on specific molecular interactions between the receptor and sequences of DNA known as hormone responsive elements (HRE) (Alberts 2002). It is triggered by hormone binding to the NRs, and involves formation of large macromolecular complexes that include coactivator and corepressor proteins. The NRs recognize both hormones and HREs in a highly selective fashion (Ribeiro et al. 1995; Weatherman et al. 1999; Togashi et al. 2005; Alberts 2002; Kumar and Thompson 1999).

NRs are composed of three main domains: the N-terminal region, which is largely unstructured and the least conserved within the superfamily, harbors an important transactivation function known as AF1. A bulk of experimental evidence indicates that AF1 modulates cell-specific and promoter-specific transcription (Yen 2001; Kumar and Thompson 1999). The second NR domain is the DNA binding domain (DBD), responsible for the recognition of HREs. The DBD is also involved in dimer stabilization (Ribeiro et al. 1998, 1995; Weatherman et al. 1999; Lazar 1993). The C-terminal region contains the ligand binding domain (LBD), which, as

its name suggests, recognizes and binds specific hormones. It also plays critical roles in dimerization, cofactor recruitment, and in gene transactivation and silencing (Yen 2001; Togashi et al. 2005; Kumar and Thompson 1999). Understanding ligand affinity and recognition by the LBD is of major importance for pharmaceutical design.

Thyroid hormone receptors (TR) regulate the transcription of several genes related to embriony and postnatal development of eyes, ears and the brain (Lazar 1993; Forrest et al. 1996; Fraichard et al. 1997; Gauthier et al. 1999; Ng et al. 2001). TRs influence several important physiological processes related to alert state such as heart frequency and metabolic rates, affecting body weight, and circulating cholesterol, lipoprotein and triglycerides levels (Baxter et al. 2004; Johansson et al. 2005). The known natural TR ligands are 3,5,3′-triiodo-L-thyronine (thyronine or T3), 3,5,3′,5′-tetra-iodothyronine (thyroxine or T4), and Triac. There are two major TR isoforms, α (TRα) and β (TRβ), which, in humans, are encoded by the NR1A1 and NR1A2 genes located in chromosomes 3 and 17, respectively (Wagner et al. 2001). TR isoforms are found in different concentrations in different tissues. TRα is highly expressed in the heart, skeletal muscle and brown fat tissues and its activation is associated with observed modifications in cardiac behavior and loss of bone and muscle masses (Lazar 1993; Wagner et al. 2001). TRβ is predominantly found in the liver and its activation is associated with increasing metabolic rates and energy consumption, resulting in weight loss and reduction of blood plasma lipid levels (Baxter et al. 2004; Johansson et al. 2005; Ye et al. 2003). Both subtypes present approximately the same affinity (around 10^{-10} M) and

activation responses to T3. Thus, increasing T3 levels can result in beneficial results due to TRβ activation, but also evoke undesirable deleterious responses resulting from activation of TRα. Therefore, developing synthetic thyromimetics that act as β-selective TR modulators is of great pharmacological interest (Togashi et al. 2005; Baxter et al. 2004; Johansson et al. 2005; Wagner et al. 2001; Yoshihara et al. 2003).

The 3D structures of TR LBDs are composed of twelve α-helices (H1–H12) and four small β-strands, a fold that is mostly conserved between NRs' LBDs. The binding cavity is deeply buried within the hydrophobic core of the LBD and is almost completely filled by the ligand. The binding pockets of TRα and TRβ are composed of several hydrophobic amino acids and by two polar regions, as depicted in Fig. 1a. A single histidine located in H11 forms one of the polar interactions: a hydrogen bond with the phenolic hydroxyl of the outer thyronine ring of agonist ligands. Most polar ligand interactions, however, are formed with three arginine residues located on H3 and on the β-strands, and by a serine in TRα or an asparagine in TRβ, as shown in Fig. 1b. The polar interactions of the ligand with this region of the protein depends on an intricate hydrogen bond network which involves surrounding water molecules (Martínez et al. 2006, 2009). However, the high affinity of TR ligands is mostly dependent on their hydrophobicity, as their thyronine rings are stabilized by a series of non-polar interactions (Fig. 1b).

The binding pocket of TRs is mostly conserved between TRα and TRβ, with the exception of Ser277 in TRα being substituted by an asparagine (Asn331) in TRβ. Many high affinity ligands are known, and the crystal structures are

Fig. 1 a Description of TR binding site in terms of polar and non-polar residues. Non-polar residues, which largely constitute the binding pocket, are shown in *light gray*, whereas polar residues are shown *black*. b General aspect of agonist ligands and their interactions with binding pocket residues. The ligand's polar head and tail interacts with the few polar residues in the binding site. The hydrophobic body interacts with a large number of non-polar residues
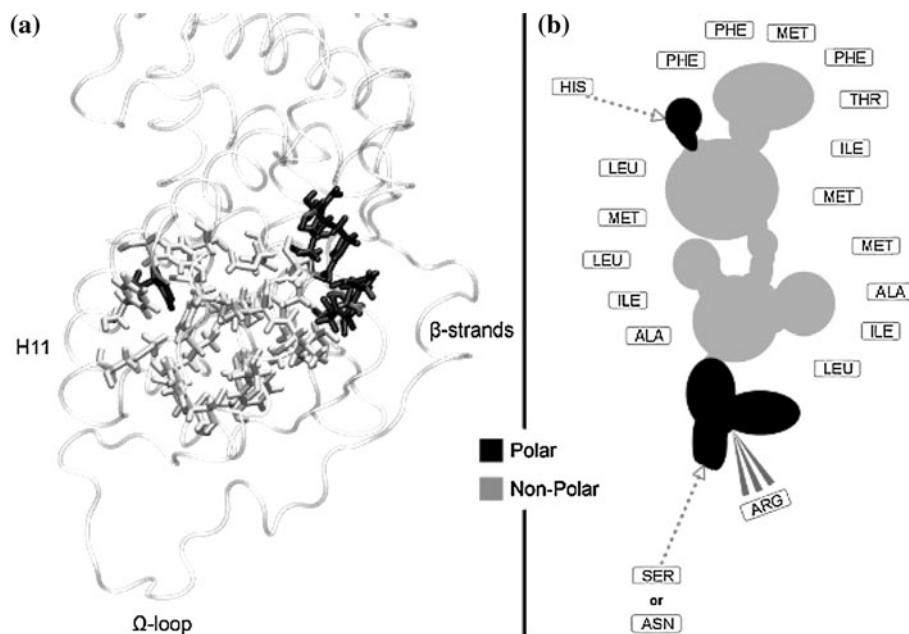
available for T3, KB141, GC1 and Triac with both iso-forms, and for GC24 with TRβ. With the exception of GC24, which bears a large hydrophobic tail in position 5′, the structural scaffold of the other ligands is essentially the same. Nevertheless, their affinities and isoform selectivities vary, and in most cases the reasons for these differences remain unclear in spite of wealth of structural information. Molecular modeling of the ligand–LBD complexes have been a valuable tool for the elucidation of these differences and revealed an unexpected diversity of mechanisms (Martínez et al. 2009; Bleicher et al. 2008).

For example, the structural specificities conferring β-selectivity for GC1 can be tracked down to the Ser/Asn mutation and its effect on the hydrogen bonding network of the carboxylic head of the ligand (Bleicher et al. 2008). Selectivity arises mostly from the removal of the amino group of T3 in GC1, which causes the displacement of the backbone of the Asn or Ser residues towards the binding pocket (Fig. 2a, b). While in TRβ the backbone of the Asn residue is still able to form strong interactions with the Arg282, the corresponding interaction in TRα (with Arg228) is partially lost due to the shorter Ser277 chain. This results in an overall less stable binding pocket.

The larger side-chain of the Asn331 residue relative to the Ser277 can also explain partially the β-selectivity of KB141 (Ye et al. 2003). The polar head of KB141 is shortened relative to that of T3, and the amino group is also removed. This shortened polar head results in unstable interactions of the ligand's carboxylate with Arg228 in TRα, as shown in Fig. 2c. Similarly to GC1, however, the longer side-chain of the Asn331 residue in TRβ indirectly stabilizes an Arg282 conformation that can interact with KB141, thus favoring binding to TRβ (Fig. 2d).

While the ability of the Asn331 side chain to stabilize "productive" Arg282 conformations seems to be an important factor towards β-selectivity of GC1 (Bleicher et al. 2008), very distinct mechanisms were observed for other ligands. For example, recent crystallographic models and molecular dynamics simulations have shown that Triac (Martínez et al. 2009), which bears a polar head identical to the one of KB141, acquires β-selectivity by a completely different mechanism. The crystal structures indicate that Triac interacts more strongly with TRα. Simulations have shown that this was indeed the case, but that entry of water molecules in the TRβ binding pocket compensates these favorable TRα bonds, resulting in similar overall interaction energies. Triac then displays improved flexibility in TRβ, suggesting an entropic gain towards to β-selectivity (Martínez et al. 2009). Finally, another striking example of the diversity of binding modes comes from the GC24 ligand. It contains a polar head identical to that of GC1, and the crystal structure of the TRβ–GC24 complex displays conformations similar to those of GC1 in this part of
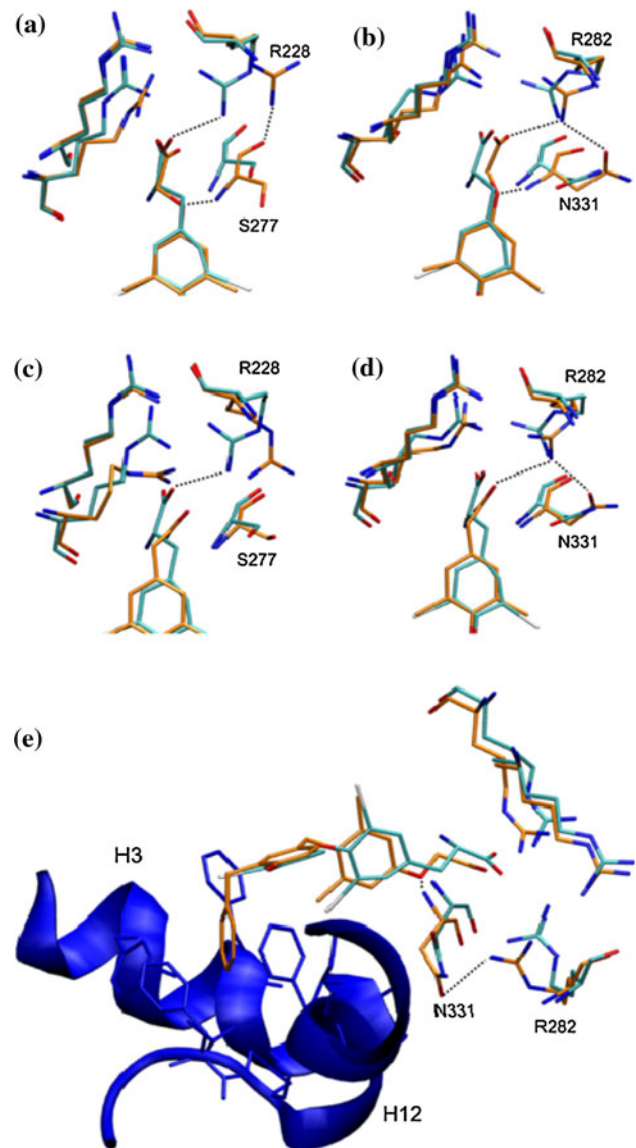

Fig. 2 Comparison of the crystallographic binding modes of T3 (*cyan*) with those of β-selective ligands (*orange*). **a** and **b** correspond to the binding modes of GC1 to TRα and TRβ, respectively. **c** and **d** to the binding modes of KB141 to TRα and TRβ. Binding of GC24 to TRβ is shown in (**e**). For GC1 and KB141, different ligand properties result in more stable binding to TRβ due to the indirect stabilization of R282–ligand interactions promoted by the Asn331 side chain. GC24 accommodates a bulky 5′ extension within helices 3 and 12, conferring additional β-selectivity

the binding pocket, as illustrated in Fig. 2e (Borngraeber et al. 2003). However, it also contains a large 5′ phenyl extension in the opposite side of the ligand which is accommodated within Helices 3 and 12 of the TRβ LBD. This confers additional selectivity towards TRβ, which apparently has greater conformational plasticity than the TRα subtype.

Many other synthetic derivatives are known to activate TR with wide ranges of binding affinities and isoform

selectivities. Our molecular level understanding of the affinities of such ligands remains very limited due to the lack of the corresponding holo-LBD crystal structures, thus motivating molecular modeling studies. In the context of nuclear receptors, molecular dynamics (MD) simulations have been reported focusing on structural variations and conformational adaptations of LBD mutants (Carlsson et al. 2005), ligand–LBD interactions (Martínez et al. 2009; Bleicher et al. 2008), and dynamics of ligand binding (Martínez et al. 2008) and dissociation (Blondel et al. 1999; Carlsson et al. 2006; Celik et al. 2007, 2008; Genest et al. 2008; Kosztin et al. 1999; Martínez et al. 2005, 2006; Peräkylä 2009; Sonoda et al. 2008).

In this work we use a well-known docking program combined with MD simulations in order to propose structural models for the binding of several high-affinity ligands to the LBDs of both TRα and TRβ isoforms, for which there are no known crystallographic structures available so far. The models, thus, generated provide for the first time insights into the binding modes of structurally quite distinct TR agonists and help elucidating the molecular reasons for their binding affinities and isoform selectivity. MD simulations are performed on the proposed structures and the ligand binding free energies are estimated within the linear interaction energy (LIE) approximation (Nam et al. 2003; Oostenbrink et al. 2000; Oostenbrink and van Gunsteren 2005; Stjernschantz et al. 2006; van Lipzig et al. 2004), showing reasonable agreement with experimental values. Given the limitations of the LIE approximation, it would be desirable to further validate the docked structures with more elaborate binding free energy calculations. However, this is beyond the scope of the present study.

In "Theoretical and computational details" we summarize the theoretical framework and details of the calculations. In "Results and discussion" we present the structural models we obtain and discuss their relevance in terms of the comprehension of TR ligand recognition and pharmacological implications. Concluding remarks are presented in last section.

Theoretical and computational details

Two sets of ligands are considered in this study: a "training-set", composed of ligands for which crystallographic models are available (Table 1), and a "model-set" of ligands for which structural models are being proposed. The training-set is composed by five ligands shown in Fig. 3, and models are proposed for other eight ligands with unknown structures, which are represented in Fig. 4. Experimental binding affinities for all these ligands are known. Our primary goal is to obtain biophysically sensible structural models for the model-set ligands which can

Table 1 Crystal structures used in MD simulations of the training set

Isoform	Ligand	PDB-ID	Isoform	Ligand	PDB-ID
α	GC1	3HZF	β	GC1	3IMY
α	IH5	1NAV	β	IH5	1NAX
α	T3	2H77	β	T3	2H6 W
α	Triac	3JZB	β	Triac	3JZC
			β	GC24	1Q4X

IH5 and KB141 are used interchangeably here to specify the same ligand

serve as a first-time view of their binding modes within the ligand binding pockets of TR.

Parameterization of ligands

The molecular models for the ligands pertaining to the training set were taken from our previous study (Martínez et al. 2005) and the parameterization of the model-set ligands was performed using the same methodology. All molecules were treated as fully flexible. Bonded and van der Waals interaction potential parameters were obtained by group analogy from the CHARMM force field (MacKerell et al. 1998), except the ones for iodine atoms, which were taken from our previous T3 model (Martínez et al. 2005). The partial atomic charges of the model set ligands were obtained from *ab initio* quantum chemical calculations consistent with the protein force field performed with Gaussian03 (Frisch et al. 2004). Calculations for molecules without iodine atoms were performed at the RHF/6-31G** level of theory and Merz–Kollman (MK) charges. Since iodine atoms are not described by 6-31G** basis set and do not support MK fitting of the electrostatic surface potential, iodine containing ligands were parameterized at the MP2/LanL2DZ level of theory and Mulliken partial charges (Martínez et al. 2005). All ligand parameters are supplied as supplementary material.

Docking

Docking calculations were performed using GOLD v3.0.1 (CCDC 2007) in order generate initial ligand–LBD structures for complexes with no crystallographic structures available (model-set). GOLD utilizes a genetic algorithm (GA) to perform the pose of the compound into the protein active site. The genetic algorithm parameters to determine this operation were automatically defined by GOLD based on pre-defined parameter settings built from a diversified test-set of ligands and proteins. The active site was defined as the region within 10 Å radius from the nearly central carbon of the co-crystallized ligand. GOLD has two built-in score functions. The default fitness function GoldScore

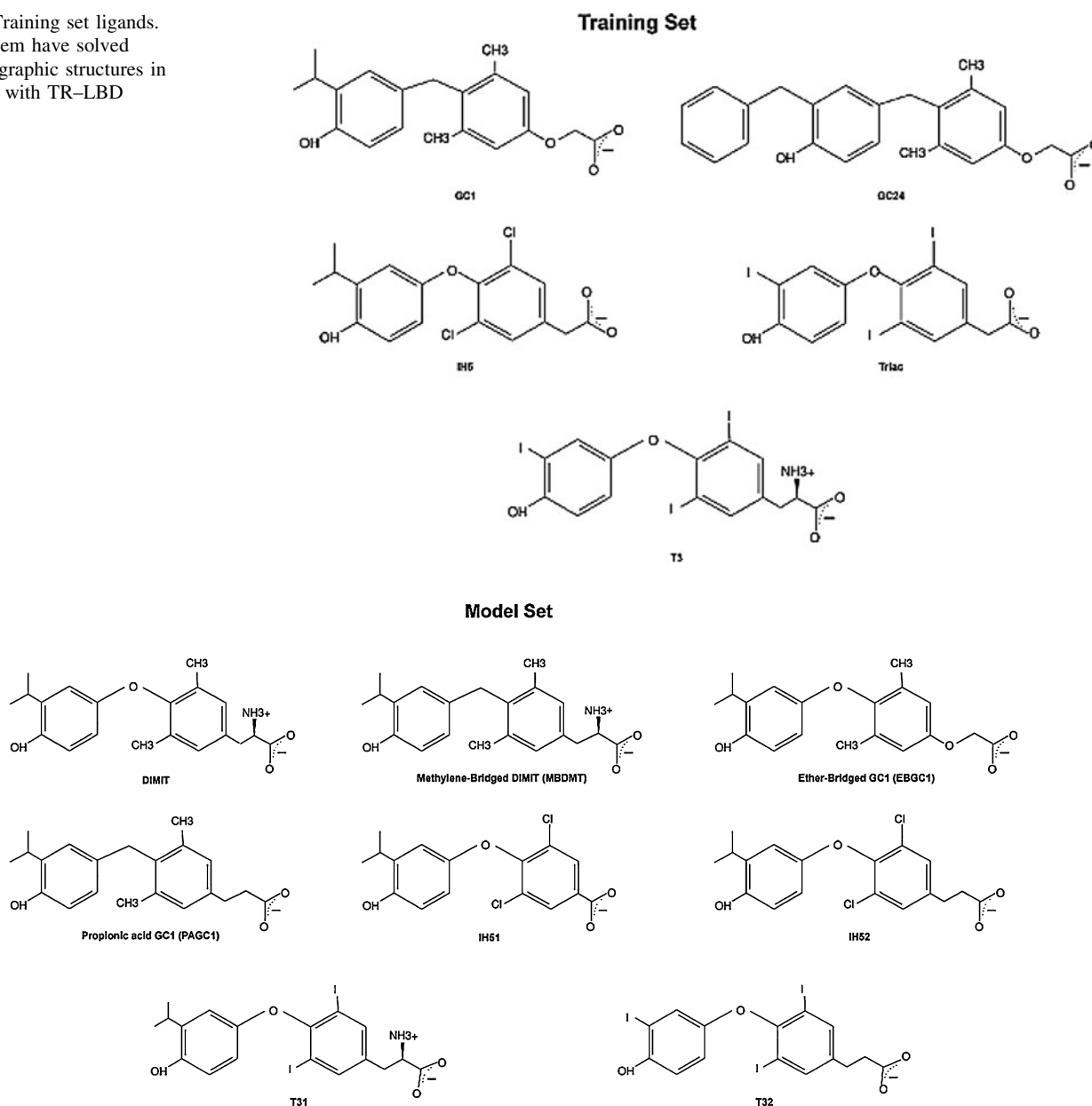**Fig. 3** Training set ligands. All of them have solved crystallographic structures in complex with TR–LBD

Training Set

GC1

GC24

IH5

Triac

T3

Model Set

DIMIT

Methylene-Bridged DIMIT (MBDMT)

Ether-Bridged GC1 (EBGC1)

Propionic acid GC1 (PAGC1)

IH51

IH52

T31

T32

Fig. 4 High affinity test set ligands. Every ligand in this group has been derived from some training set ligand and present K_D to TRβ under 10 nM

consists of four components (protein–ligand hydrogen bond energy, protein–ligand van der Waals interaction energy, ligand internal van der Waals energy, and ligand torsional strain energy). The ChemScore scoring function was derived empirically from a set of 82 protein–ligand complexes for which measured binding affinities were available. Unlike GoldScore, the ChemScore function was trained by regression against the reported affinity data. Because the two scoring functions emphasize different aspects of the ligand–protein coupling, we have employed both functions to evaluate the posing procedure. GOLD was set to output up to 10 best conformations after each

run. From these computationally evaluated sets, we choose the best ranked pose within those that were consistent with general aspects of ligand orientation in the binding pocket.

Different protein targets were chosen according to availability of known ligands and diversity of binding-site properties: the four co-crystallized structures of hTRα and hTRβ available on PDB containing T3 and IH5 ligands were retrieved (Codes: 2H77 and 2H6W for T3 (Nascimento et al. 2006), and 1NAV and 1NAX for IH5 (Ye et al. 2003)). The co-crystallized structures of hTRα and hTRβ with GC1 were recently obtained in our lab (Bleicher et al. 2008) with PDB IDs 3HZF and 3IMY, respectively. These

structures were processed in order to remove ligands and water molecules. The compounds GC1, IH5 and T3 were extracted from the proteins files and used as the other ligands in docking and calculations steps, so that they could be used to monitor the accuracy of the results. Ligands without crystallographic structures available were built with the Sybyl (Sybyl 2005). Hydrogen atoms were added to all ligands and their Tripos force field energies (Clark et al. 1989) were minimized.

Molecular dynamics simulations

MD simulations were performed using the NAMD package (Phillips et al. 2005) with CHARMM force field parameters for the protein (MacKerell et al. 1998) and TIP3P for water (Jorgensen et al. 1983). We used the crystal structures displayed in Table 1 for the simulations of the training-set. For simulating the ligands in solution, we built 40 Å wide cubic boxes containing a single ligand molecule, approximately 2,000 water molecules and sodium and chloride ions in order to render the systems electrically neutral. Simulations for ligand–LBD complexes were performed with 80 Å wide cubic boxes, nearly 15,000 water molecules and sufficient sodium and chloride ions for electroneutrality. The systems' energies were minimized by 500 conjugate-gradient steps. All MD simulations were performed in NPT ensemble at 298 K and 1 atm, with periodic boundary conditions, using a time step of 2 fs and constraining all covalent bonds involving hydrogen atoms to the corresponding equilibrium positions. The van der Waals interactions were cutoff at 15 Å with a switching function starting at 12 Å. The electrostatic interactions were treated using the particle mesh Ewald (PME) method (Darden et al. 1993) with the following parameters: tolerance 10^{-6}, Ewald real space coefficient 0.219398, grid dimensions $81 \times 81 \times 81$ Å³, and maximum grid spacing 1.5 Å. PME electrostatics were used for generating the dynamics but not to compute the average ligand–surroundings interaction energy needed for estimating the binding affinities (see below). For each system, the energy minimized structure was equilibrated by a 1 ns simulation, followed by 500 ps runs from which interaction energies were evaluated by pair-wise sums of van der Waals and Coulomb interactions between the ligand its surroundings (Eq. 1).

Linear interaction energy

The LIE method provides approximate estimates to the absolute binding and hydration free energies with low computational effort. Within this approximation, the ligand–protein binding free energy is given by

$$\Delta G_{\text{Bind}} = \beta\big(\langle V_{l-s}^{\text{el}}\rangle_{\text{bound}} - \langle V_{l-s}^{\text{el}}\rangle_{\text{free}}\big) + \alpha\big(\langle V_{l-s}^{\text{vdw}}\rangle_{\text{bound}} - \langle V_{l-s}^{\text{vdw}}\rangle_{\text{free}}\big) + \gamma, \tag{1}$$

where $\langle V_{l-s}^{\text{el}}\rangle_Y$ and $\langle V_{l-s}^{\text{vdw}}\rangle_Y$ are the average values of the electrostatic and van der Waals interactions between the ligand (l) and its surroundings (s) in the ligand state Y, which can be either *free* in solution or *bound* to the protein. The α and β parameters are, respectively, dispersion and electrostatic adjustable energy scale factors and γ is a constant term dependent of ligand or binding site hydrophobicity and accessible surface-area (Hansson et al. 1998). Recent developments of the method have shown that reasonable LIE free energy estimates for a given ligand–protein system require calibrating the energy and hydrophobicity parameters to the particular system of interest by tuning α, β and γ in order to reproduce the experimental binding free energies of a group of ligands named training-set (Stjernschantz et al. 2006; Bren et al. 2006; Ganguly and Mukhopadhyay 2006; Tounge et al. 2006; Raineri et al. 2005). The optimized set of parameters is subsequently utilized to estimate the binding free energy of other ligands, usually referred to as the test set. Calibration of parameters has been performed for TRα and TRβ separately, but the adjusted parameter values turned out only slightly dependent on TR isoform.

Here, we assembled the training set with ligands for which holo-LBD crystallographic structures are available. These ligands are shown in Fig. 3. All training set ligands are agonists and have high affinity to TR, showing the general structural features described in Fig. 1b: a phenol, a highly polar carboxylate, and a hydrophobic body. The experimental dissociation constant (K_D), the binding free energies obtained from these K_D values, and the TR isoform selectivity of each ligand are shown in Table S1 of the supplemental material (Ye et al. 2003; Yoshihara et al. 2003; Martínez et al. 2009; Borngraeber et al. 2003; Chiellini et al. 1998; Nguyen et al. 2002). The endogen ligand T3 has approximately the same affinity to both LBD isoforms, while the exogen ones (GC1, GC24, IH5 and Triac) are all β-selective.

Binding free energy estimates were obtained from the proposed structural models. This group of ligands, shown in Fig. 4, have experimental dissociation constants in the nanomolar range, thus being high-affinity synthetic TR ligands and, consequently, relevant for ligand design. GC24 was included in the model-set for TRα since no crystallographic structure for the TRα–GC24 complex is available. Experimental K_D's from which free energies were derived are shown in Table S2 of supplemental material (Ye et al. 2003; Yoshihara et al. 2003; Borngraeber et al. 2003). The β-selectivity of the ligands are correlated with that of their parents, ranging from the

Table 2 Ligand-neighborhood non-bonded interaction energies for free and bound states obtained from MD simulations for high affinity ligands for TRα and TRβ isoforms

	Ligand	β-selectivity	$\langle V_{\text{Free}}^{\text{el}} \rangle$	$\langle V_{\text{Bound}}^{\text{el}} \rangle$	$\langle V_{\text{Free}}^{\text{vdW}} \rangle$	$\langle V_{\text{Bound}}^{\text{vdW}} \rangle$	ΔV^{el}	ΔV^{vdw}
TRα (TRβ)								
Training-set	T3	1.00	−143.03	−89.73	−26.97	−50.20	53.30	−23.23
				(−95.75)		(−48.14)	(47.28)	(−21.17)
	Triac	6.00	−183.57	−160.23	−28.90	−47.26	23.34	−18.36
				(−160.27)		(−46.60)	(23.30)	(−17.70)
	IH5	11.11	−164.59	−136.70	−23.32	−43.79	27.89	−20.47
				(−146.67)		(−44.42)	(17.92)	(−21.10)
	GC1	8.52	−173.85	−179.24	−22.86	−44.38	−5.39	−21.52
				(−165.99)		(−47.33)	(7.86)	(−24.47)
	GC24	33.81	−177.56	–	−27.66	–	–	–
				(−186.56)		(−48.67)	(−9.00)	(−21.01)
Model-set	T31	0.62	−166.83	−81.43	−24.91	−52.43	85.40	−27.52
				(−89.96)		(−50.90)	(76.87)	(−25.99)
	T32	1.00	−193.85	−169.74	−30.24	−51.39	24.11	−21.15
				(−171.37)		(−51.26)	(22.48)	(−21.02)
	IH51	3.03	−157.47	−159.74	−21.97	−39.94	−2.27	−17.97
				(−153.62)		(−39.77)	(3.85)	(−17.80)
	IH52	2.47	−170.53	−158.19	−23.94	−44.09	12.34	−20.15
				(−170.97)		(−43.94)	(−0.44)	(−20.00)
	DIMIT	1.07	−118.80	−88.91	−23.49	−43.03	29.89	−19.54
				(−96.62)		(−39.84)	(22.18)	(−16.35)
	EBGC1	5.21	−174.38	−189.99	−22.18	−40.70	−15.61	−18.52
				(−175.48)		(−44.16)	(−1.10)	(−21.98)
	MBDMT	1.25	−120.35	−72.93	−23.31	−47.17	47.42	−23.86
				(−84.04)		(−46.16)	(36.31)	(−22.85)
	PAGC1	2.45	−181.70	−180.06	−22.14	−43.95	1.64	−21.81
				(−176.69)		(−45.53)	(5.01)	(−23.39)
	GC24	33.81	−178.10	−171.65	−28.02	−48.19	6.45	−20.17
				–		–	–	–

Selectivity of each ligand is obtained from K_a-TRβ/ K_a-TRα, normalized by K_a-TRβ/ K_a-TRα for T3. All energies are in kcal/mol

Table 3 LIE parameters for the training-sets of ligands for TRα and TRβ

	TRα	TRβ
α	0.42	0.45
β	0.01	0.01
γ/kcal mol^{-1}	−4.00	−4.00

most β-selective ligand GC24 to the weakly α-selective ligand T31.

Ligand–surroundings non-bonded average interaction energies for the model set ligands are shown in Table 2. The LIE parameters were obtained by least-square fitting the LIE equation to the experimental binding free energies and are listed in Table 3 for TRα and TRβ, respectively. The low value of the electrostatic β parameter may reflect the low polarity of the ligands and the fact that the important ligand–protein hydrophilic contacts in the binding pocket are nearly compensated by ligand–water interactions in solution (Martínez et al. 2006), thus masking the role of the electrostatic interactions in the LIE calculations. The replacement of ligand–protein hydrophilic contacts by ligand–solvent interactions has been suggested to facilitate ligand dissociation from the binding pocket through the β-sheet region (Martínez et al. 2006). Small β (∼0.06) has also been found in the context of other nuclear receptors (Stjernschantz et al. 2006). Table 4 lists the calculated and experimental binding free energies for each ligand considered. Scatter plots of the experimental and calculated binding free energies for the model set ligands to both isoforms are depicted in Fig. 5. The agreement is fairly reasonable given the rather approximate nature of the LIE method. The root mean square deviations from the ideal

Table 4 Calculated and experimental binding free energies of high affinity ligands with both isoforms

		TRα		TRβ	
		ΔG_{calc}	ΔG_{exp}	ΔG_{calc}	ΔG_{exp}
Training-set	T3	−13.22	−13.53	−13.05	−13.69
	Triac	−11.48	−13.86	−11.73	−14.04
	KB141	−12.32	−11.25	−13.32	−12.83
	GC1	−13.09	−12.28	−14.93	−13.70
	GC24	–	–	−13.54	−13.54
		RMS = 0.98 kcal mol^{-1}		RMS = 1.26 kcal mol^{-1}	
Model-set	T31	−14.70	−14.32	−14.93	−14.18
	T32	−12.64	−15.04	−13.23	−15.22
	IH51	−11.57	−10.27	−11.97	−11.07
	IH52	−12.34	−13.31	−13.00	−14.00
	DIMIT	−11.91	−11.00	−11.14	−11.19
	EBGC1	−11.93	−11.75	−13.90	−12.87
	MBDMT	−13.55	−11.85	−13.92	−12.13
	PAGC1	−13.14	−12.49	−14.48	−13.16
	GC24	−12.41	−10.73	–	–
		RMS = 1.31 kcal mol^{-1}		RMS = 1.24 kcal mol^{-1}	

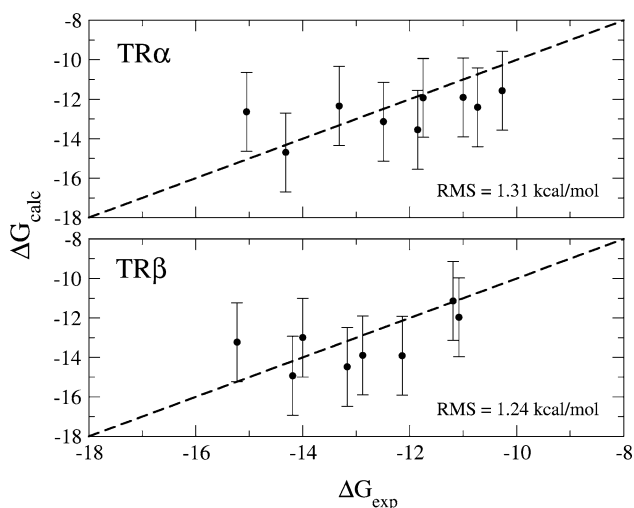All energies are in kcal/mol

Fig. 5 Calculated versus experimental binding free energies for the model-set ligands to TRα and TRβ isoforms. All values are in kcal/mol. The error bars for ΔG_{calc} were calculated from the average energy values obtained from the simulations. Experimental errors for ΔG_{exp} are roughly estimated at 0.2 and 0.4 kcal/mol for TRα and TRβ from different T3 binding affinity data (see Supporting information)

behavior (dashed lines) are only 1.31 and 1.24 kcal/mol for TRα and TRβ, respectively. The correlation factor between ΔG_{calc} and ΔG_{exp} is low ($R \sim 0.54$). However, there are too few data points for each TR isoform for a meaningful quality assessment of the calculated free energies in terms of this parameter.

Results and discussion

Structural models of ligand–LBD complexes were built for the eight high affinity ligands (Fig. 4) bound to both α and β isoforms, and for GC-24 bound to TRα. Figures 6 and 7 display the average structures from MD simulations of the modeled ligands (orange) superimposed with the crystal structure most relevant for each comparison (cyan). Models built on TRα and TRβ are displayed in left and right panels, respectively, except for the TRα–GC24 model, which is superimposed with the TRβ-GC24 crystal structure. The structures depicted here were produced to indicate the most relevant differences in the binding modes of the structural models. The corresponding PDB files of the docked conformations are available as supplementary material. The most important structural features of each ligand–LBD complex and an analysis of their relevance follows.

DIMIT

The DIMIT ligand (Fig. 4) shares the hydrophobic body with GC1 and the polar head with T3. Its affinity to both isoforms is reduced relative to the ones of T3 and GC1 (refer to Table 4 for binding free energies), and it is slightly β-selective. The structural models obtained were able to reproduce this reduced affinity with good precision (Table 4): deviations relative to experimental values being −0.91 and 0.05 kcal mol^{-1} for TRα and TRβ, respectively.
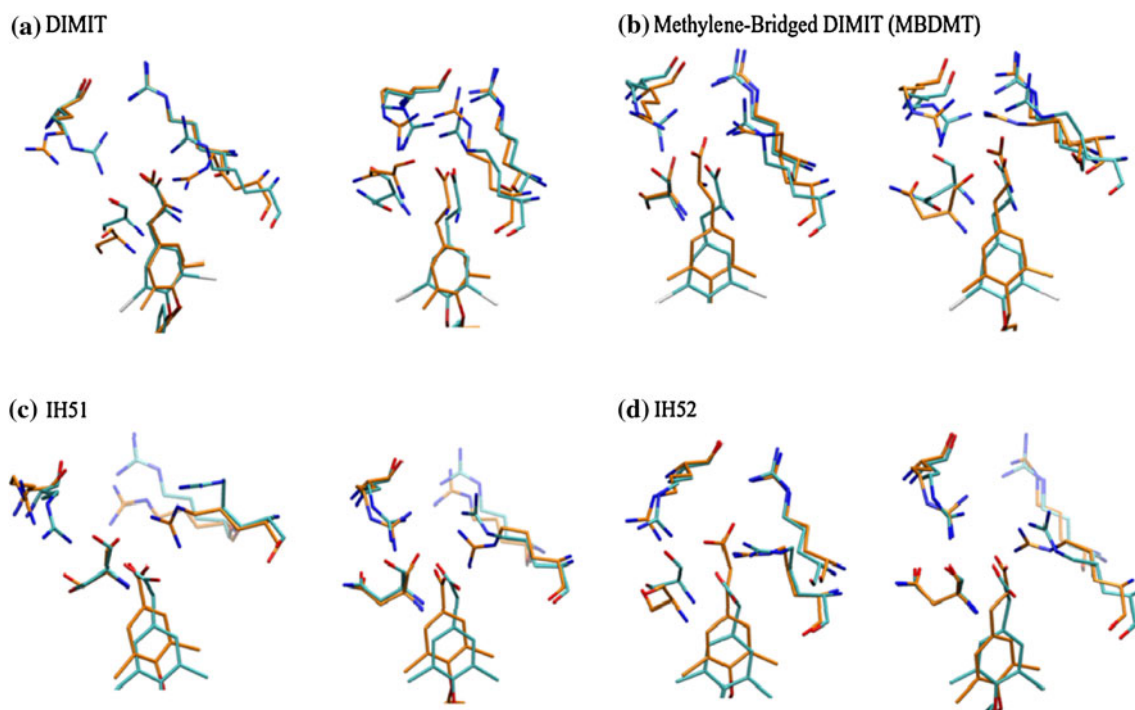
Fig. 6 Structural models (*orange*) compared to relevant crystal structures (*cyan*) for models built on TRα (*left*) or TRβ (*right*). **a** Modeled DIMIT superimposed with the crystal structure of the TR–T3 complexes. **b** The methylene-bridged DIMIT model compared to TR-T3. **c** IH51–TR and **d** IH52–TR complex models superimposed with the KB141 crystal structure. Models are shown in *orange* and crystal structures are shown in *cyan*

The structural models of DIMIT bound to TRα and TRβ are shown in Fig. 6a. In TRα, DIMIT is oriented in the binding pocket similarly to T3, but with some aromatic ring twisting which, in turn, do not seem to significantly affect the position of the hydrophobic pocket residues (not shown). In contrast, the binding mode of the polar head changes, with the side chains of arginines 228 and 262 switching their roles at interacting directly with the ligand's carboxylate. There is also a significant displacement of the Ser277 residue, as observed for GC1 (Fig. 2a). This displacement was attributed to the removal of the amino group in GC1 relative to T3 (see discussion above), but the docking of this ligand indicates that it may occur even in the presence of this group if the hydrophobic portion of the ligand is similar to that of GC1. Nevertheless, there is no comparable gain in β-selectivity.

The DIMIT binding mode in TRβ is more preserved relative to T3 (Fig. 6a, right panel). The positions of the arginines are mostly preserved and, whereas there is some displacement of the ligand in the binding pocket, it is hard to discern any qualitative effect of these movements in the hydrophobic cavity. The side-chain of Asn331 is shifted towards Arg282 and looses its interactions with DIMIT's amino group, thus suggesting a mechanism for the reduced affinity.

In summary, the docking of this ligand indicates that even if the amino-group of T3 is kept, some indirect effect

of the hydrophobic body of the ligand contributes to the altered Asn/Ser interactions relative to T3 and which are observed for GC1 (Bleicher et al. 2008).

Methylene-bridged DIMIT

MBDMT is also a slightly β-selective ligand, with reduced affinity towards both isoforms relative to T3 or GC1. The only difference it bears relative to DIMIT is the substitution of the ether oxygen bridging the two aromatic rings by a methylene group. It is well known that this ether oxygen does not form any clearly discernible hydrophilic interactions in the binding pocket, and its effect on ligand affinity and selectivity is still poorly understood. We have some indications that differences in selectivity between MBDMT and DIMIT may largely arise from the additional torsional restraints the oxygen atom introduces to relative orientation of the two rings (Souza et al., unpublished). The modeled complexes (Fig. 6b) reveal that in TRα the ligand was significantly displaced relative to the position of T3. The positions of the polar groups of the binding pocket were not significantly altered, and only small rotations of the side-chains of arginines 228 and 262 were observed. Similar conformational adaptations were observed for TRβ, with the additional displacement of the side chain of Asn331. These binding modes may not be considered with the same detail as the ones for DIMIT because of the greater

inaccuracy of the binding free-energies (see Table 4; "Methylene-bridged DIMIT"). Nevertheless, the results indicate that the removal of the ether oxygen facilitates the displacement of the ligand in the binding pocket; hence, the formation of favorable interactions, consistently with its improved affinity relative to DIMIT.

IH51

The IH51 ligand is similar to KB141, but one additional methylene group is removed from the polar head of the molecule. This results in decreased affinity to both isoforms when compared to KB141, and a significant loss in β-selectivity. The experimental binding free-energies of IH51 are reproduced with deviations of -1.3 and -0.9 kcal mol^{-1}, for TRα and TRβ, respectively. The binding models (Fig. 6c) are interesting in the sense that the ligand seems to react to the shortened polar chain by simply moving within the binding pocket towards the arginines. The interactions with the arginines seem to be strengthened relative to KB141, with greater proximity of Arg262 and Arg266 in TRα and of the corresponding Arg316 and Arg320 in TRβ (in TRα, however, Arg228 moves away from the ligand's carboxylate). The decreased affinity of IH51 relative to KB141, therefore, does not seem to arise from reduced polar interactions, as one might have expected, but from reduced hydrophobic interactions resulting from the displacement of the ligand towards the most hydrophilic portion of the pocket. With the exception of the Arg228/Arg282 residues, the binding modes seem to be mostly similar in either isoform, consistently with the reduced β-selectivity.

IH52

Contrary to IH51, IH52 is a modification of the KB141 ligand in which an additional methylene group is added to the carboxylate tail. This results in increased affinity towards TRα and TRβ, but with lower β-selectivity. The calculated binding affinities turned out 0.97 and 1.00 kcal mol^{-1} higher than experimental values for TRα and TRβ isoforms, respectively. The modeled binding mode of IH52 in TRα (Fig. 6d) resembles in some ways the binding mode of IH51, with the ligand being displaced towards the polar portion of pocket relative to KB141. By doing so, IH52 is able to interact with the three arginines of the binding pocket, which essentially have the same orientation as in the TRα–KB141 crystal structure. In contrast, this dislocation of the ligand seems to require the displacement of the Ser277 backbone, which now interacts less tightly with Arg228. At the same time, the ligand in TRβ is orientated in the binding pocket almost identically to KB141, the same occurring for the arginines and the Asn331 residue. A small rotation of the

Arg262 side chain favors its interaction with the ligand's carboxylate. The longer carboxylate chain facilitates the interaction of this group with the polar part of the binding pocket in both TRα and TRβ, thus favoring binding relative to KB141, in agreement to the experimental affinities. Accordingly, the more constrained TRα binding pocket (as inferred from crystallographic temperature factors) appears to implicate in the displacement of the backbone of Ser277 residue, which may explain the (small) β-selectivity of this ligand.

Ether-bridged GC1

The EBGC1 ligand is an analog of GC1 in which the methylene group linking the aromatic rings is substituted by an ether oxygen. This results in decreased affinity to both TRα and TRβ relative to GC1. The experimental binding free-energies of these ligands were reproduced with deviations of -0.18 and -1.03 kcal mol^{-1} for TRα and TRβ. As already pointed out, the ether oxygen does not interact directly with any polar group in the binding pocket, and its substitution by a methylene group seems to increase affinity by reducing a conformational constraint (Souza et al., unpublished). Coherently, the binding mode obtained for TRα was almost identical to that of GC1, and the binding free-energy was accurately reproduced. For TRβ, on the other hand, the predicted affinity is higher than the observed one, and this can be attributed to a stronger interaction with the side chain of Arg316, which has flipped in towards the carboxylate in our docking model (Fig. 7a). Therefore, EBGC1 seems to bind both TRs essentially in the same way GC1 does, and differences in affinity and selectivity arises from conformational constraints introduced by the ether bridge.

Propionic-acid GC1

The PAGC1 ligand differs from GC1 by the substitution of its ether bridge by a methylene group. This modification is located on the carboxylate head of the ligand, thus reducing its ability to form polar bonds in the binding pocket. It reduces significantly β-selectivity by slightly increasing affinity to TRα and reducing affinity to TRβ. Binding free-energies were obtained with good accuracies, with -0.65 and -1.32 kcal mol^{-1} deviations relative to experimental values for TRα and TRβ, respectively, which render the calculated affinities somewhat overestimated.

As shown in Fig. 7b, the orientation of the ligand in the binding pocket resembles that of GC1. However, whereas GC1 forms a hydrogen bond with the backbone of the Ser277 or Asn331 residues, PAGC1 cannot do so because of the substitution of the ether oxygen. This explains its reduced affinity. The lack of this hydrogen bond displaces
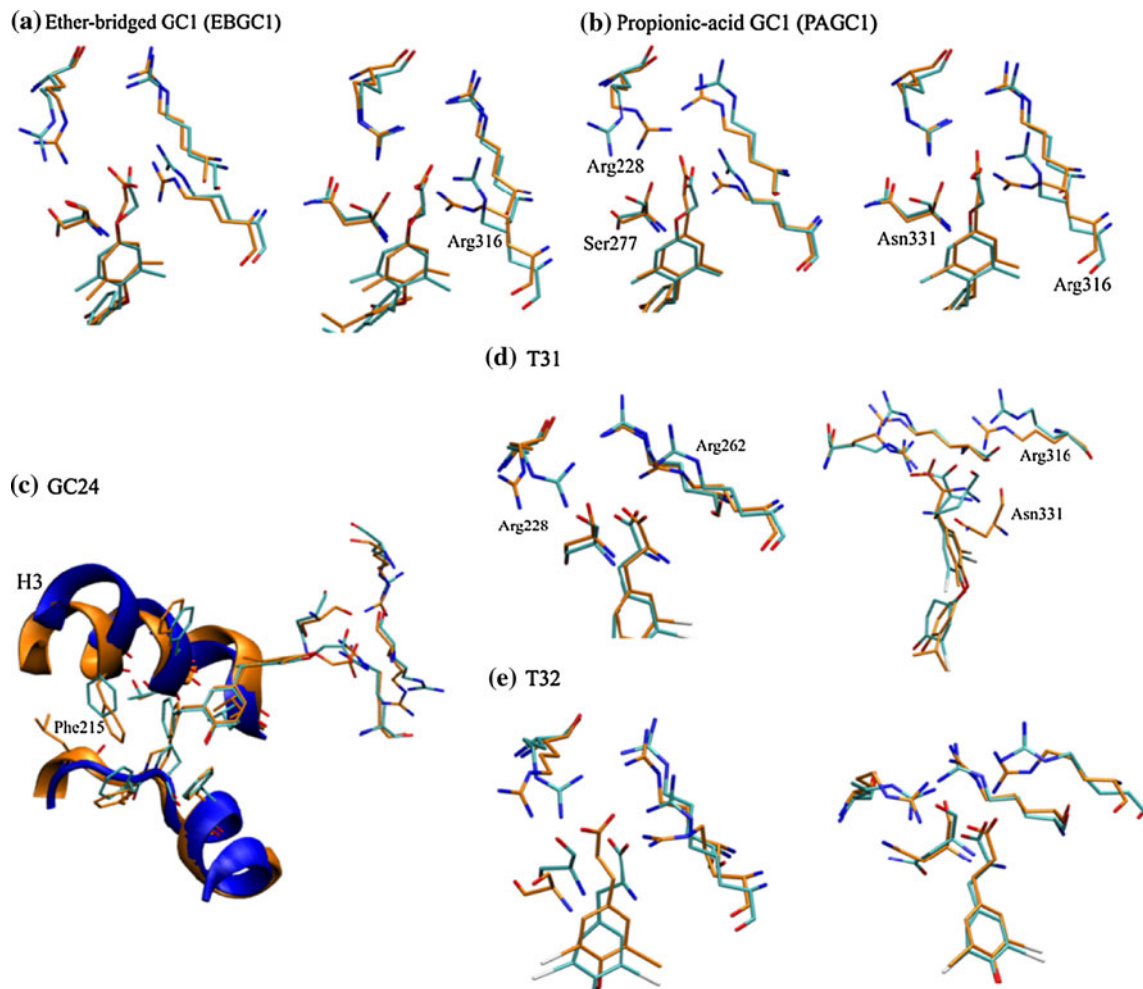
(a) Ether-bridged GC1 (EBGC1)

(b) Propionic-acid GC1 (PAGC1)

Arg228

Ser277

Asn331

Arg316

(d) T31

Arg262

Arg316

Asn331

Arg228

(c) GC24

H3

Phe215

(e) T32

Fig. 7 Structural models superimposed to relevant crystal structures for TRα (*left*) and TRβ (*right*). **a** Ether-bridged GC1 models superimposed with corresponding TR–GC1 crystal structures. **b** Propionic-acid GC1 models superimposed with TR–GC1 crystal structures. **c** Superposition of the TRα–GC24 model with the TRβ–GC24 crystal structure. Structural models of the **d** T32 and **e** T31 ligands superimposed with the LBD–T3 crystal structures. Models are shown in *orange* and crystal structures are shown in *cyan*

PAGC1 slightly away from the Ser277/Asn331 residues and allows for PAGC1 interactions with Arg228 in TRα and Arg316 in TRβ that are actually stronger than those exhibited by GC1 with these residues. The fact that these ligand–arginine interactions do not compensate the reduced ligand–Ser277/Asn331 interactions can be explained by the presence of water molecules in the binding pocket. While the interaction with the Ser/Asn residues occur deeply in the binding cavity and in a position where the ligand is tightly packed, the polar interactions of the carboxylate head can be substituted by interactions with water molecular with little or no energetic cost (Martínez et al. 2006). In this case, the absence of direct GC1–arginine interactions that appear to be present in PAGC1 are intermediated by water molecules not necessarily visible in the crystal structures. This ligand, therefore, illustrates that the loss polar interactions between ligand and binding pocket is mostly deleterious when occurring in tightly packed solvent inaccessible groups.

GC24 in TRα

GC24 is a surprising ligand containing a large 5′-hyrophobic extension that can be accommodated by the LBD of TRβ maintaining essentially the same affinity as T3. GC24 affinity towards TRα is much reduced, thus making it highly β-selective. We predicted the binding free-energy of GC24 to TRα with a deviation of −1.68 kcal mol^{-1} (affinity being again overestimated). Nevertheless, the superposition of the crystal structure of the TRβ–GC24 complex with the corresponding TRα docking model (Fig. 7c) provides for several interesting observations. First, the binding modes of the polar part of the ligand are essentially identical to those of GC1 in both isoforms, indicating that the selectivity arises

partially from the same structural reasons as for GC1 (Bleicher et al. 2008). However, additional loss of affinity to TRα may come from conformational stress observed in H3 in the presence of GC24 relative to the crystal structure of the TRβ complex. Unlike the TRβ LBD structure, whose flexibility allows for the accommodation of the 5′ extension of GC24, the modeled TRα–GC24 structure shows that the Phe215 residue in H3 (Phe269 in TRβ) experiences a significant displacement due to the interaction with the GC24 phenyl substituent.

T31 and T32

T31 and T32 are T3 analogs. In T31 the 3′ iodine of T3 is substituted by an isopropyl radical, while in T32 the amino-group is removed. T31 is curious for being the sole ligand which displays slight α-selectivity, whereas T32 is not selective. Both ligands also display improved affinities to both isoforms. In our calculations, while the affinity of T31 was accurately reproduced (deviations of -0.38 and -0.75 kcal mol^{-1}), the binding free-energy of T32 was missed by approximately 2 kcal mol^{-1}.

The models suggest that T31 binding to TRα is mostly preserved relative to T3 (Fig. 6d), with some flipping of the side chains of Arg228 and Arg262, the former loosing interactions with the ligand's carboxylate and the later augmenting them. Interactions of T31 with TRβ are modified by a significant rotation of the phenolic ring, and there is an important displacement of the Asn331 residue. This structural difference is surprising in view of the similarity between these ligands, although it follows the trend discussed above for MBDMT ligand, for which displacement of the Asn331 backbone was also observed for a hydrophobic body similar to GC1's. The structural basis for the improved affinities resulting from substituting the iodine atom by a propyl radical remains elusive. The differences in affinity seem to arise from improved ligand–protein dispersive interactions without inducing any clearly detectable side chain conformational adaptations.

The improved affinity of T32 probably comes from its increased hydrophobicity resulting from the removal of the amino group. As observed for GC1, displacement of the Ser277 residue in TRα occurs and tighter bonds to Arg residues in TRβ are clearly visible. However, we should refrain from further analysis based on the modeled structures given the inaccuracy of our binding free-energy estimates for this ligand.

Concluding remarks

In this work, structural models were obtained for several TR high-affinity ligands with unknown structures by means of a well-respected docking procedure and MD simulations. We use the structural models to gain insights into the putative binding modes of these high-affinity ligand–TR complexes and estimate their binding free energy within the approximated LIE method. Docked models and average interaction energies obtained from MD trajectories indicate that if, at the one hand, substituting the interactions of the ligand's polar head with the binding pocket residues by ligand–water interactions involves little or no energetic cost. The observed affinities, on the other hand, seem to depend on the chemical nature of the ligand's polar head in most cases. This is an indirect consequence of the fact that most ligands were designed from known leads (mostly T3, GC1 and KB141), and for which structural alterations were made in their polar head envisioning isoform selectivity by altered interactions with the Ser277/Asn331 binding pocket mutation.

Fine tuning of binding affinities at the polar interaction level seems possible, but the structural basis underlying each effect is very complex. A previously unsuspected diversity of mechanisms is progressively being observed for ligand–TR interactions, even in the cases where ligands seem to bear overall similar structural scaffolds. The crystal structures of complexes with T3, GC1, Triac, KB141 and GC24 already provided a glimpse on the complexity of these interactions. The binding modes of other high-affinity ligands, modeled here, complement this picture. For instance, we have previously attributed the movements of the Ser277/Asn331 backbones in the presence of GC1, to the absence of the amino group relative to T3 (Bleicher et al. 2008). The binding modes of DIMIT and T31 proposed here, however, suggest that these movements may be also caused by the hydrophobic body of GC1, since the presence of the amino group in DIMIT and T31 does not lead to β-selectivity. Controlling the size of the carboxylate chain of the ligands has also been used to improve protein–ligand polar head interactions. Our results show that shorter chains are capable of interfering with hydrophobic packing effects, reducing the affinity (see IH51 and IH52). Large polar heads, on the other hand, generally enhance affinity, but, alone, cannot promote isoform selectivity. The carboxylate chains of Triac and KB141, of intermediate sizes, result in intermediate affinities and binding modes that give rise to β-selectivity.

Finally, in order to elucidate the role of hydrophobic interactions in binding affinity, it is still necessary to refine the interaction models, both by generating additional and more detailed crystal structures as well as improving modeling procedures. While it is clear that these interactions are essential for the attachment of the ligands to the binding pocket, the lack of specificity is still a barrier for their understanding at the molecular level and use in rational drug design. This is illustrated particularly by the

effects of replacing the iodine by an isopropyl group in T31, which leads to α-selectivity. The molecular nature of this α-selectivity remains elusive. Apart from subtle variations in dispersive interactions, some binding effects may result from properties of the ligand charge distribution or flexibility, being the methylene-bridged and T31 thyromimetics good examples of this phenomenon.

References

Alberts B (2002) Molecular biology of the cell, 4th edn. Garland Science, New York

Baxter JD, Webb P, Grover G, Scanlan TS (2004) Selective activation of thyroid hormone signaling pathways by GC-1: a new approach to controlling cholesterol and body weight. Trends Endocr Met 15:154–157

Bleicher L, Aparicio R, Nunes FM, Martínez L, Dias SMG, Figueira ACM, Santos MAM, Venturelli WH, da Silva R, Donate PM, Neves FAR, Simeoni LA, Baxter JD, Webb P, Skaf MS, Polikarpov I (2008) Structural basis of GC-1 selectivity for thyroid hormone receptor isoforms. BMC Struc Biol 8:8

Blondel A, Renaud JP, Fischer S, Moras D, Karplus M (1999) Retinoic acid receptor: a simulation analysis of retinoic acid binding and the resulting conformational changes. J Mol Biol 291:101–115

Borngraeber S, Budny MJ, Chiellini G, Cunha-Lima ST, Togashi M, Webb P, Baxter JD, Scanlan TS, Fletterick RJ (2003) Ligand selectivity by seeking hydrophobicity in thyroid hormone receptor. Proc Nat Acad Sci USA 100:15358–15363

Bren U, Martinek V, Florian J (2006) Free energy simulations of uncatalyzed DNA replication fidelity: structure and stability of T center dot G and dTTP center dot G terminal DNA mismatches flanked by a single dangling nucleotide. J Phys Chem B 110:10557–10566

Carlsson P, Koehler KF, Nilsson L (2005) Glucocorticoid receptor point mutation V571M facilitates coactivator and ligand binding by structural rearrangement and stabilization. Mol Endocr 19:1960–1977

Carlsson P, Burendahl S, Nilsson L (2006) Unbinding of retinoic acid from the retinoic acid receptor by random expulsion molecular dynamics. Biophys J 91:3151–3161

CCDC (2007) Gold 3.0.1. Cambridge Crystallographic Data Centre, Cambridge, UK

Celik L, Lund JDD, Schiott B (2007) Conformational dynamics of the estrogen receptor alpha: molecular dynamics simulations of the influence of binding site structure on protein dynamics. Biochem 46:1743–1758

Celik L, Lund JDD, Schiott B (2008) Exploring interactions of endocrine-disrupting compounds with different conformations of the human estrogen receptor alpha ligand binding domain: a molecular docking study. Chem Res Toxicol 21:2195–2206

Chiellini G, Apriletti JW, Yoshihara HA, Baxter JD, Ribeiro RCJ, Scanlan TS (1998) A high-affinity subtype-selective agonist ligand for the thyroid hormone receptor. Chem. Biol. 1998(5):299–306

Clark M, Cramer RD, Vanopdenbosch N (1989) Validation of the general-purpose tripos 5.2 force-field. J Comp Chem 10:982–1012

Darden T, York D, Pedersen L (1993) Particle mesh Ewald—an N.Log(N) method for Ewald Sums in large systems. J Chem Phys 98:10089–10092

Forrest D, Erway LC, Ng L, Altschuler R, Curran T (1996) Thyroid hormone receptor beta is essential for development of auditory function. Nat Genet 13:354–357

Fraichard A, Chassande O, Plateroti M, Roux JP, Trouillas J, Dehay C et al (1997) The T3R alpha gene encoding a thyroid hormone receptor is essential for post-natal development and thyroid hormone production. EMBO J 16:4412–4420

Frisch MJ, Trucks GW, Schlegel HB, Scuseria GE, Robb MA, Cheeseman JR et al (2004) Gaussian 03, revision C.02. Gaussian, Inc., Wallingford CT

Ganguly D, Mukhopadhyay C (2006) Binding diversity of the two binding sites of ricin B lectin. Biopolymers 83:83–94

Gauthier K, Chassande O, Plateroti M, Roux JP, Legrand C, Pain B et al (1999) Different functions for the thyroid hormone receptors TR alpha and TR beta in the control of thyroid hormone production and post-natal development. EMBO J 18:623–631

Genest D, Garnier N, Arrault A, Marot C, Morin-Allory L, Genest M (2008) Ligand-escape pathways from the ligand-binding domain of PPAR gamma receptor as probed by molecular dynamics simulations. Eur Biophys J 37:369–379

Hansson T, Marelius J, Aqvist J (1998) Ligand binding affinity prediction by linear interaction energy methods. J Comp Aid Mol Des 12:27–35

Johansson L, Rudling M, Scanlan TS, Lundasen T, Webb P, Baxter JD et al (2005) Selective thyroid receptor modulation by GC-1 reduces serum lipids and stimulates steps of reverse cholesterol transport in euthyroid mice. Proc Nat Acad Sci USA 102:10297–10302

Jorgensen WL, Chandrasekhar J, Madura JD, Impey RW, Klein ML (1983) Comparison of simple potential functions for simulating liquid water. J Chem Phys 79:926–935

Kosztin D, Izrailev S, Schulten K (1999) Unbinding of retinoic acid from its receptor studied by steered molecular dynamics. Biophys J 76:188–197

Kumar R, Thompson EB (1999) The structure of the nuclear hormone receptors. Steroids 64:310–319

Lazar MA (1993) Thyroid-hormone receptors—multiple forms, multiple possibilities. Endocr Rev 14:184–193

MacKerell AD, Bashford D, Bellott M, Dunbrack RL, Evanseck JD, Field MJ et al (1998) All-atom empirical potential for molecular modeling and dynamics studies of proteins. J Phys Chem B 102:3586–3616

Martínez L, Sonoda MT, Webb P, Baxter JD, Skaf MS, Polikarpov I (2005) Molecular dynamics simulations reveal multiple pathways of ligand dissociation from thyroid hormone receptors. Biophys J 89:2011–2023

Martínez L, Webb P, Polikarpov I, Skaf MS (2006) Molecular dynamics simulations of ligand dissociation from thyroid hormone receptors: evidence of the likeliest escape pathway and its implications for the design of novel ligands. J Med Chem 49:23–26

Martínez L, Polikarpov I, Skaf MS (2008) Only subtle protein conformational adaptations are required for ligand binding to thyroid hormone receptors: simulations using a novel multipoint steered molecular dynamics approach. J Phys Chem B 112:10741–10751

Martínez L, Nascimento AS, Nunes FM, Phillips K, Aparicio R, Dias SMG et al (2009) Gaining ligand selectivity in thyroid hormone

receptors via entropy. Proc Natl Acad Sci USA 106:20717–20722

Nam K, Marshall P, Wolf RM, Cornell W (2003) Simulation of the different biological activities of diethylstilbestrol (DES) on estrogen receptor alpha and estrogen-related receptor gamma. Biopolymers 68:130–138

Nascimento AS, Dias SM, Nunes FM, Aparicio R, Ambrosio ALB, Bleicher L et al (2006) Structural rearrangements in the thyroid hormone receptor hinge domain and their putative role in the receptor function. J Mol Biol 360:586–598

Ng L, Hurley LB, Dierks B, Srinivas M, Salto C, Vennstrom B et al (2001) A thyroid hormone receptor that is required for the development of green cone photoreceptors. Nat Genet 27:94–98

Nguyen NH, Apriletti JW, Lima STC, Webb P, Baxter JD, Scanlan TS (2002) Rational design and synthesis of a novel thyroid hormone antagonist that blocks coactivator recruitment. J Med Chem 45:3310–3320

Oostenbrink C, van Gunsteren WF (2005) Free energies of ligand binding for structurally diverse compounds. Proc Nat Acad Sci USA 102:6750–6754

Oostenbrink C, Pitera JW, van Lipzig MMH, Meerman JHN, van Gunsteren WF (2000) Simulations of the estrogen receptor ligand-binding domain: affinity of natural ligands and xenoestrogens. J Med Chem 43:4594–4605

Peräkylä M (2009) Ligand unbinding pathways from the vitamin D receptor studied by molecular dynamics simulations. Eur Biophys J 38:185–198

Phillips JC, Braun R, Wang W, Gumbart J, Tajkhorshid E, Villa E et al (2005) Scalable molecular dynamics with NAMD. J Comp Chem 26:1781–1802

Raineri FO, Stell G, Ben-Amotz D (2005) New mean-energy formulae for free energy differences. Mol Phys 103:3209–3221

Ribeiro RCJ, Kushner PJ, Baxter JD (1995) The nuclear hormone-receptor gene superfamily. Annu Rev Med 46:443–453

Ribeiro RCJ, Apriletti JW, Wagner RL, Feng WJ, Kushner PJ, Nilsson S et al (1998) X-ray crystallographic and functional studies of thyroid hormone receptor. J Steroid Biochem 65:133–141

Sonoda MT, Martínez L, Webb P, Skaf MS, Polikarpov I (2008) Ligand dissociation from estrogen receptor is mediated by receptor dimerization: evidence from molecular dynamics simulations. Mol Endocr 22:1565–1578

Souza PCT, Martínez L, Polikarpov I, Skaf MS (2009) In preparation

Stjernschantz E, Marelius J, Medina C, Jacobsson M, Vermeulen NPE, Oostenbrink C (2006) Are automated molecular dynamics simulations and binding free energy calculations realistic tools in lead optimization? An evaluation of the linear interaction energy (LIE) method. J Chem Info Mod 46:1972–1983

Sybyl (2005) Version 7.1. Tripos Inc.

Togashi M, Borngraeber S, Sandler B, Fletterick RJ, Webb P, Baxter JD (2005) Conformational adaptation of nuclear receptor ligand binding domains to agonists: potential for novel approaches to ligand design. J Steroid Biochem 93:127–137

Tounge BA, Rajarnani RT, Baxter EW, Reitz AB, Reynolds CH (2006) Linear interaction energy models for beta-secretase (BACE) inhibitors: role of van der Waals, electrostatic, and continuum-solvation terms. J Mol Graph Mod 24:475–484

van Lipzig MMH, ter Laak AM, Jongejan A, Vermeulen NPE, Wamelink M, Geerke D, Meerman JHN (2004) Prediction of ligand binding affinity and orientation of xenoestrogens to the estrogen receptor by molecular dynamics simulations and the linear interaction energy method. J Med Chem 47:1018–1030

Wagner RL, Huber BR, Shiau AK, Kelly A, Lima STC, Scanlan TS et al (2001) Hormone selectivity in thyroid hormone receptors. Mol Endocr 15:398–410

Weatherman RV, Fletterick RJ, Scanlan TS (1999) Nuclear-receptor ligands and ligand-binding domains. Annu Rev Biochem 68:559–581

Ye L, Li YL, Mellstrom K, Mellin C, Bladh LG, Koehler K et al (2003) Thyroid receptor ligands. 1. Agonist ligands selective for the thyroid receptor beta(1). J Med Chem 46:1580–1588

Yen PM (2001) Physiological and molecular basis of thyroid hormone action. Physiol Rev 81:1097–1142

Yoshihara HAI, Apriletti JW, Baxter JD, Scanlan TS (2003) Structural determinants of selective thyromimetics. J Med Chem 46:3152–3161